V European Conference on Computational Fluid Dynamics
ECCOMAS CFD 2010
J. C. F. Pereira and A. Sequeira (Eds)
Lisbon, Portugal,14-17 June 2010

THE EFFECT OF VORTEX FINDER DIAMETER ON CYCLONE SEPARATOR PERFORMANCE AND FLOW FIELD

Khairy Elsayed*, Chris Lacor†

*Vrije Universiteit Brussel, Department of Mechanical Engineering,
Research Group Fluid Mechanics and Thermodynamics, Pleinlaan 2, B-1050 Brussels, Belgium,
e-mail: khairy.elsayed@vub.ac.be
†Vrije Universiteit Brussel, Department of Mechanical Engineering,
Research Group Fluid Mechanics and Thermodynamics, Pleinlaan 2, B-1050 Brussels, Belgium
e-mail: chris.lacor@vub.ac.be

Key words: Cyclone separator, Cyclone performance, Reynolds stress model (RSM), Discrete phase modeling (DPM), Cyclone geometry, Vortex finder diameter

Abstract. *The flow pattern and performance of a cyclone, with different vortex finder diameters, was evaluated to examine the effect of the vortex finder diameter on the performance and velocity profile. Three vortex finder diameters were simulated computationally to compare the cyclone pressure drop, the cut-off size and the flow pattern of the cyclone at Reynolds number 2.8E5 (based on the inlet velocity and cyclone diameter). The three values of the vortex finder diameters are $D_x = d_x/D$=0.5, 0.4 and 0.3 where d_x is the vortex finder diameter and D is the cyclone diameter.*

The collection efficiency of the narrow vortex finder is higher than that of the wider ones but at the cost of pressure drop. The flow pattern and velocity profiles of the narrowest cyclone are quiet different from that of the other two cyclones, especially close to and through the vortex finder. Also the inner vortex becomes more asymmetric with more fluctuations in the axial direction.

1 INTRODUCTION

Cyclones are one of the most widely used separators, which rely on centrifugal forces to separate particles from a gas stream. The primary advantages are economy, simplicity in construction, and adaptable to a wide range of operating conditions, such as high temperatures and pressures. Usually, large-scaled cyclones are used to remove particles for industrial control, while small-scaled cyclones are used to separate particles for ambient and source sampling.

Reversed flow cyclones, with a tangential inlet, are the most common cyclone design as shown in Fig. 1, and consist of seven main geometrical parameters: inlet section height a and width b, cylinder height h, cyclone total height H_t, dust exit diameter (cone-tip diameter) B_c, gas exit diameter (vortex finder diameter) d_x and vortex finder height S. All

these parameters always given as a ratio of the cyclone body diameter D, It is generally known that these seven dimensions characterize the collection efficiency and pressure drop of a cyclone, and determine their cut-off diameter.[1–9] The vortex finder size is an especially important dimension, which significantly affects the cyclone performance as its size plays a critical role in defining the flow field inside the cyclone, including the pattern of the outer and inner spiral flows. Saltzman and Hochstrasser[1] studied the design and performance of miniature cyclones for repairable aerosol sampling, each with a different combination of three cyclone cone lengths and three vortex finder diameters. Iozia and Leith[4] optimized the cyclone design parameters, including the vortex finder diameter, to improve the cyclone performance using their optimization program. Kim and Lee[10] described how the ratio of the diameters of cyclone body D and the vortex finder d_x affected the collection efficiency and pressure drop of cyclones, and proposed an energy-effective cyclone design. Moore and Mcfarland[7] also tested cyclones, with six different vortex finders, and concluded that the variation in the vortex finder diameter under the constraint of a constant cyclone Reynolds number produced a change in the aerodynamic particle cut-off diameter. Recently Hoekstra[11] investigated the effect of D_x on the velocity profile using 2D axisymmetric simulation. Lim et al.[12] examined experimentally the effect of vortex finder shape on the collection efficiency at different flow rates but without any explanation on its effect of the flow field pattern and velocity profiles. Raoufi et al.[13] duplicated numerically the same study of Lim et al.[12] with limited details about the effect of the vortex finder diameter on the flow field pattern and velocity profile.

The purpose of this computational study is to help in understanding the effect of reducing the vortex finder diameter on the cyclone performance (pressure drop and cut-off size), flow pattern and velocity profile. Three cyclones with three different vortex finders diameters have been simulated and compared.

2 Numerical Simulation

2.1 Configuration of the three cyclones

The cyclone used in this study had a reversed flow tangential inlet, and the geometry and dimensions are shown in Fig. 1(a) and Table 1. Three cyclones with different vortex finder diameter are used viz., D_x= 0.5, 0.4 and 0.3. The three cyclones are identical to those used by Hoekstra[11] with a 2D axi-symmetric simulation. Nine plotting sections are used to investigate the effect of d_x on the velocity profiles as given by Fig. 1(b)and Table 2.

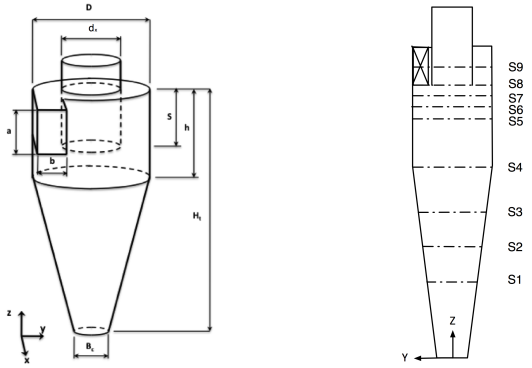

(a) Geometry (b) Sections

Figure 1: Schematic diagram for cyclone separator and positions of different plotting sections

2.2 Numerical settings

FLUENT is a commercially available CFD code which utilities the finite volume formulation to carry out coupled or segregated calculations (with reference to the conservation of mass, momentum and energy equations). For the turbulent flow in cyclones, the key to the success of CFD lies with the accurate description of the turbulent behavior of the flow.[14] To model the swirling turbulent flow in a cyclone separator, there are a number of turbulence models available in FLUENT. These range from the standard $k-\varepsilon$ model to the more complicated Reynolds stress model (RSM) and Large Eddy Simulation (LES). The $k-\varepsilon$ model involves the solution of transport equations for the kinetic energy of turbulence and its dissipation rate and the calculation of a turbulent contribution to the viscosity at each computational cell. The standard $k-\varepsilon$, RNG $k-\varepsilon$ and Realizable $k-\varepsilon$ models were not optimized for strongly swirling flows found in cyclones.[15]

The Reynolds stress turbulence model (RSM) requires the solution of transport equations for each of the Reynolds stress components. The Reynolds stress turbulence model yields an accurate prediction of the swirl flow pattern, axial velocity, tangential velocity and pressure drop in cyclone simulations.[16]

The air inlet velocity equals 10 $[m/s]$ (inlet volume flow rate Q_{in}=0.0841 $[m^3/s]$), air density 1.0 $[kg/m^3]$ and dynamic viscosity of 1.0E-5$[Pa\ s]$, leading to a Reynolds number of 2.8E5 based on the cyclone diameter and the area averaged inlet velocity. The turbulence intensity equals 4% and the turbulence characteristic length equals 0.07 times the inlet width.

The finite volume method has been used to discretize the partial differential equations of the model using the SIMPLEC (Semi-Implicit Method for Pressure-Linked Equations-Consistent) method for pressure velocity coupling and QUICK scheme to interpolate the variables on the surface of the control volume. The implicit coupled solution algorithm was selected. The unsteady Reynolds stress (RSM) turbulence model was used in this study with a time step of 0.001 [s].

Table 1: The geometrical dimensions of the three cyclones[§]

Dimension		Length (cm)	Dimension ratio (dimension/D)
Body diameter, D		29	1
Inlet height, a		14.5	0.5
Inlet width, b		5.8	0.2
Cyclone height, H_t		116	4.0
Cylinder height, h		43.5	1.5
Gas outlet duct length, S		14.5	0.5
Cone tip-diameter, B_c		10.788	0.372
Gas outlet diameter,d_x	Cyclone I	**14.5**	**0.5**
	Cyclone II	**11.6**	**0.4**
	Cyclone III	**8.7**	**0.3**

[§] The outlet section is above the cyclone surface by 0.5 D, While the inlet section located at a distance 0.75 D.

The numerical grids of cyclones I, II and III contain 392622, 389520 and 379348 hexahedral cells respectively, to yield a reasonable prediction. These runs were performed on an eight node CPU Opteron 64 Linux cluster.

3 Results and discussion

3.1 Validation of results

In order to validate the obtained results, it is necessary to compare the prediction with experimental data. Comparison was made between the present simulation and the measured axial and tangential velocity profiles (presented by Hoekstra[11] using a Laser Doppler Anomemetry (LDA) system) at axial station located at 94.25 cm from the cyclone bottom (Section S6, Fig. 1, Table 2) for Cyclone I ($D_x = 0.5$), Fig. 2. The RSM simulation predicts a similar trend as observed experimentally although the maximum tangential

Table 2: The position of different sections[§]

Section	S1	S2	S3	S4	S5	S6	S7	S8	S9
z[cm]	29	43.5	58	72.5	87	94.25	97.875	101.5	108.75
z/D	0.16	0.32	0.48	0.65	0.97	1.29	1.61	1.94	2.26

[§] Sections S1, S2 and S3 are located in the conical section. Section S4 at the end of the cylindrical part.
Sections S5, S6 and S7 located below the vortex finder inlet. S8 at the vortex finder inlet and S9 through the inlet section.

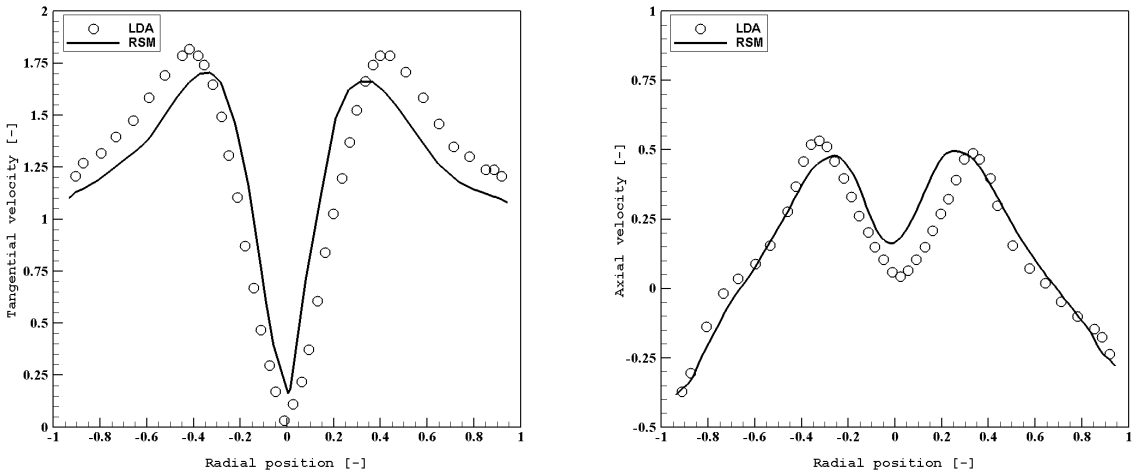

Figure 2: Comparison of the time averaged tangential and axial velocity between the LDA measurements, Hoekstra[11] and the current RSM results at section S6. From left to right tangential velocity and axial velocity, D_x=0.5.

velocity is underestimated whereas the axial velocity is overestimated in the central region. Considering the complexity of the turbulent swirling flow in the cyclones, the agreement between the simulations and measurements is considered to be quite acceptable.

3.2 Flow field pattern

3.2.1 The pressure field

Figure 3 shows the contour plot at Y=0 and also at section S9 (at the middle of inlet section). In the three cyclones the time-averaged static pressure decreases radially from wall to center. A negative pressure zone appears in the forced vortex region (central region) due to high swirling velocity. The pressure gradient is largest along the radial direction, while the gradient in axial direction is very limited. The cyclonic flow is not symmetrical as is clear from the shape of the low pressure zone at the cyclone center (twisted cylinder). The highest pressure is found for Cyclone III , implying it also has the maximum pressure drop (as the pressure at the center of cyclone outlet is fixed to atmospheric pressure). The highest pressures for cyclones I and II are very close. The central region of the cyclone is more twisted in case of cyclone III ($D_x = 0.3$).

3.2.2 The velocity field

Based on the contour plots of the time averaged tangential velocity, Fig 3, and the radial profiles at sections S1 through S9 shown in Figs. 4, 5, and 6, the following comments can be drawn. The contour plots for the tangential velocity are close to that for the absolute

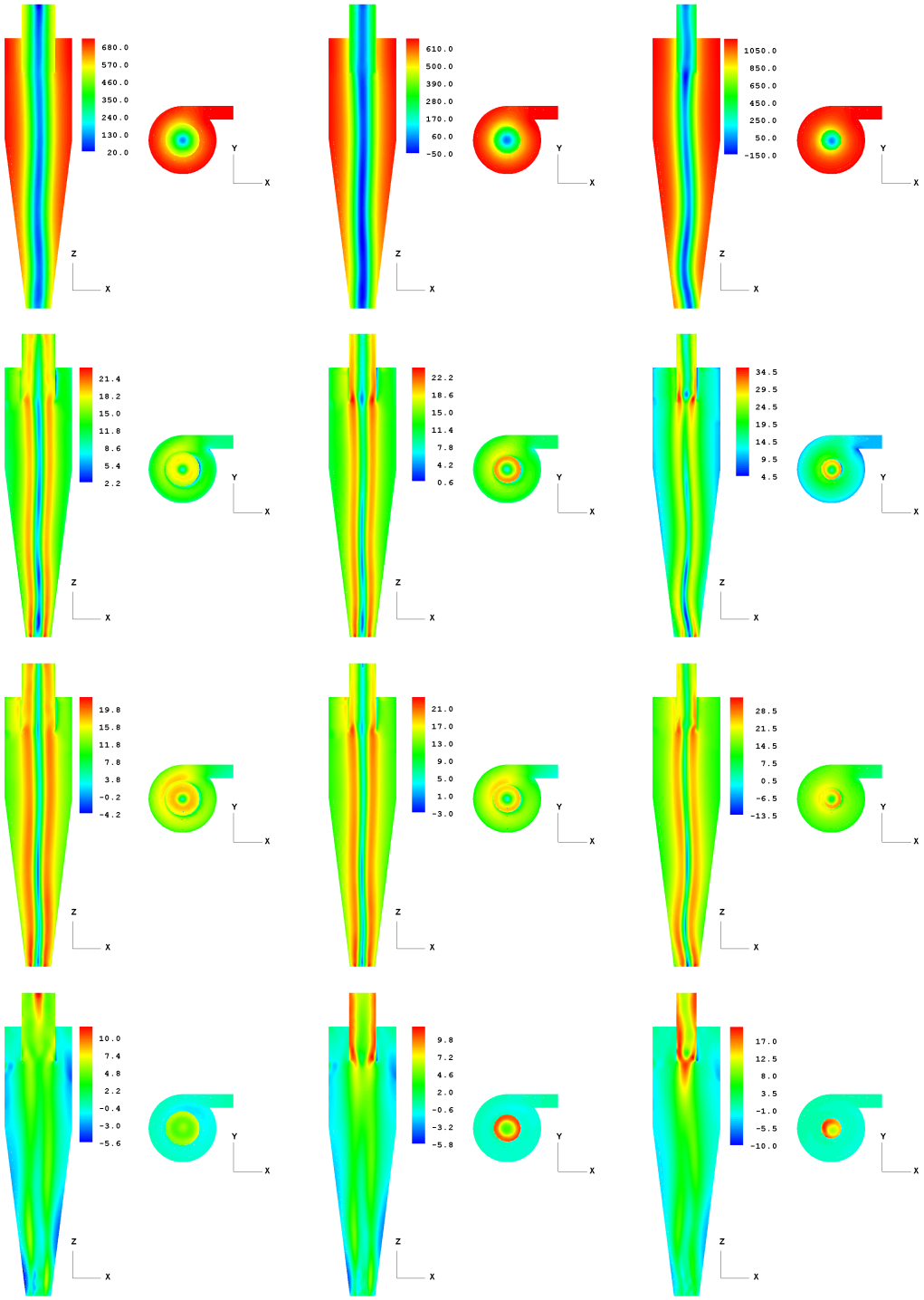

Figure 3: The contour plots for the time averaged flow variables at sections Y=0 and S9. From top to bottom: static pressure [N/m^2], absolute velocity [m/s], tangential velocity [m/s] and axial velocity [m/s]. From left to right $D_x = 0.5$, $D_x = 0.4$ and $D_x = 0.3$ respectively.

velocity, indicating the tangential velocity is the dominant velocity component. The maximum tangential velocity may reach 2.8 times the average inlet velocity and occurs in the annular cylindrical part in case of cyclone III. The tangential velocity distribution for the three cyclones are nearly identical in pattern, with the highest velocity occurring in case of Cyclone III. The tangential velocity profile at any section is composed of two regions, an inner and an outer one. In the inner region the flow rotates approximately like a solid body (forced vortex), where the tangential velocity increases with radius. After reaching its peak the velocity decreases with radius in the outer part of the profile (free vortex). This profile is a so-called Rankine type vortex, including a quasi-forced vortex in the central region and a quasi-free vortex in the outer region.

The radial profiles given in Figs. 4, 5, 6 represent the time averaged tangential and axial velocity in the nine sections for each cyclone. Starting at section S1 near the cyclone bottom and moving upward, there is a clear difference between the velocity profile of cyclone III ($D_x = 0.3$) and that of cyclones I and II both for tangential and axial velocity. The ratio between the maximum tangential velocity for $D_x = 0.3$ and that for both $D_x = 0.4, 0.5$ is between 1.4 close to the cyclone bottom and 1.57 close to the vortex finder. The forced vortex region is narrower in case of $D_x = 0.3$ and has the shape of a twisted cylinder. In general, the difference between the tangential velocities for cyclones I and II are small.

The axial velocity contours indicate there are two flow streams, Fig 3. A downward flow directed towards the cyclone bottom (negative axial velocity), and an upward flow directed towards the vortex finder exit. The axial velocity reaches maximum either close to the position of maximum tangential velocity or close to the cyclone center in case of cyclone III away from cyclone bottom. The axial velocity profiles shown in Figs. 4, 5, 6 exhibit a severe asymmetrical feature. The axial velocity profile for cyclone III is completely different than that of the other two cyclones especially in the cylindrical portion of the cyclone.

Figure 7 depicts the flow behavior at the cyclone center along the axial direction for the three cyclones. The axial profile of the tangential velocity of cyclone I and II is quite similar (close to zero) whereas cyclone III shows a fluctuation behavior (between unity and negative one-half of the inlet velocity). With increasing the axial distance, the axial velocity profile behaves quite differently for the three cyclones.

3.3 Discrete phase modeling (DPM)

The Lagrangian discrete phase model in FLUENT follows the Euler-Lagrange approach. The fluid phase is treated as a continuum by solving the time-averaged Navier-Stokes equations, while the dispersed phase is solved by tracking a large number of par-

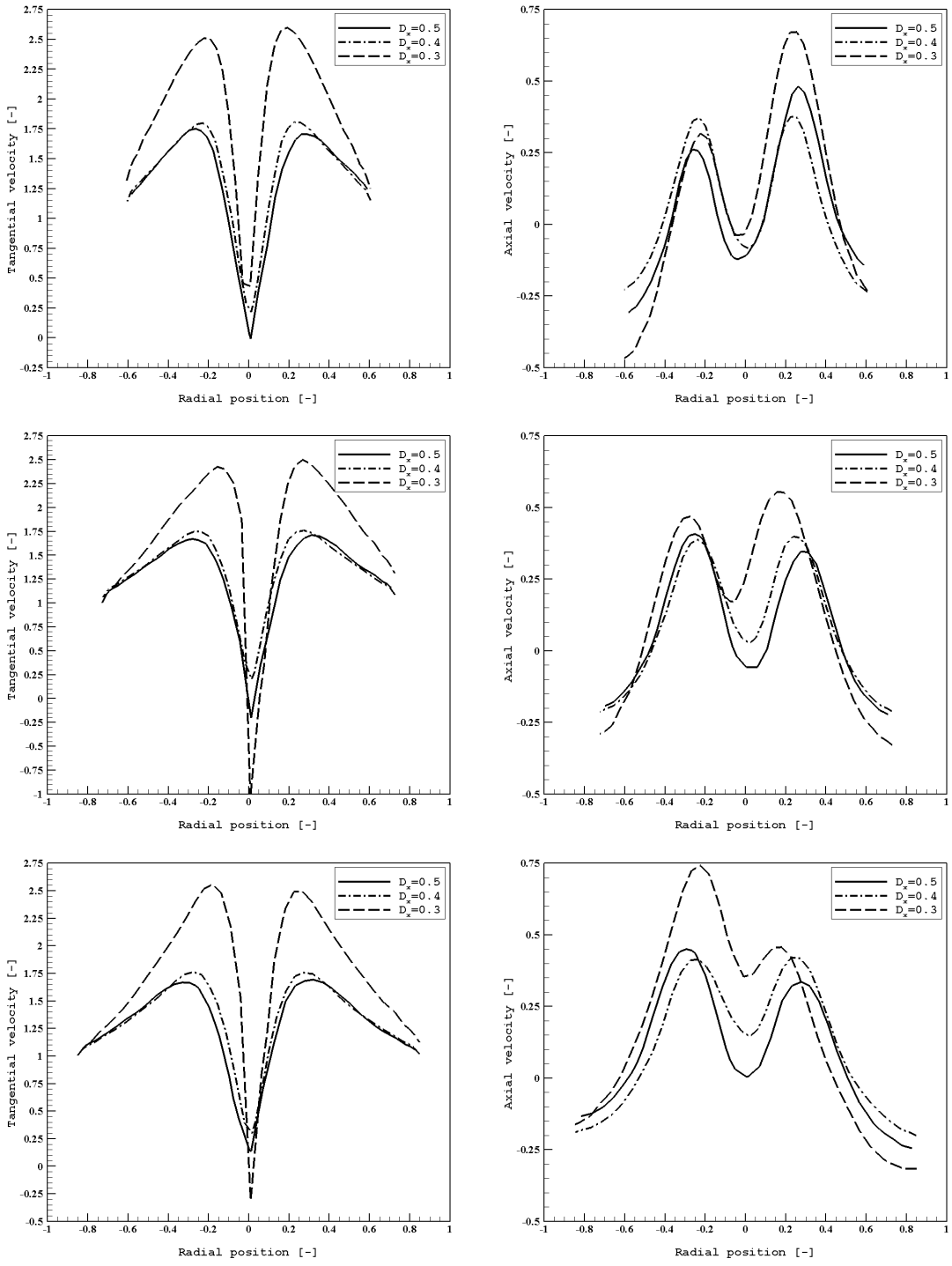

Figure 4: The radial profile for the time averaged tangential and axial velocity at different sections on the X-Z plane (Y=0) at sections S1 till S3 . From top to bottom: section S1 through section S3. From left to right: tangential velocity and axial velocity respectively.

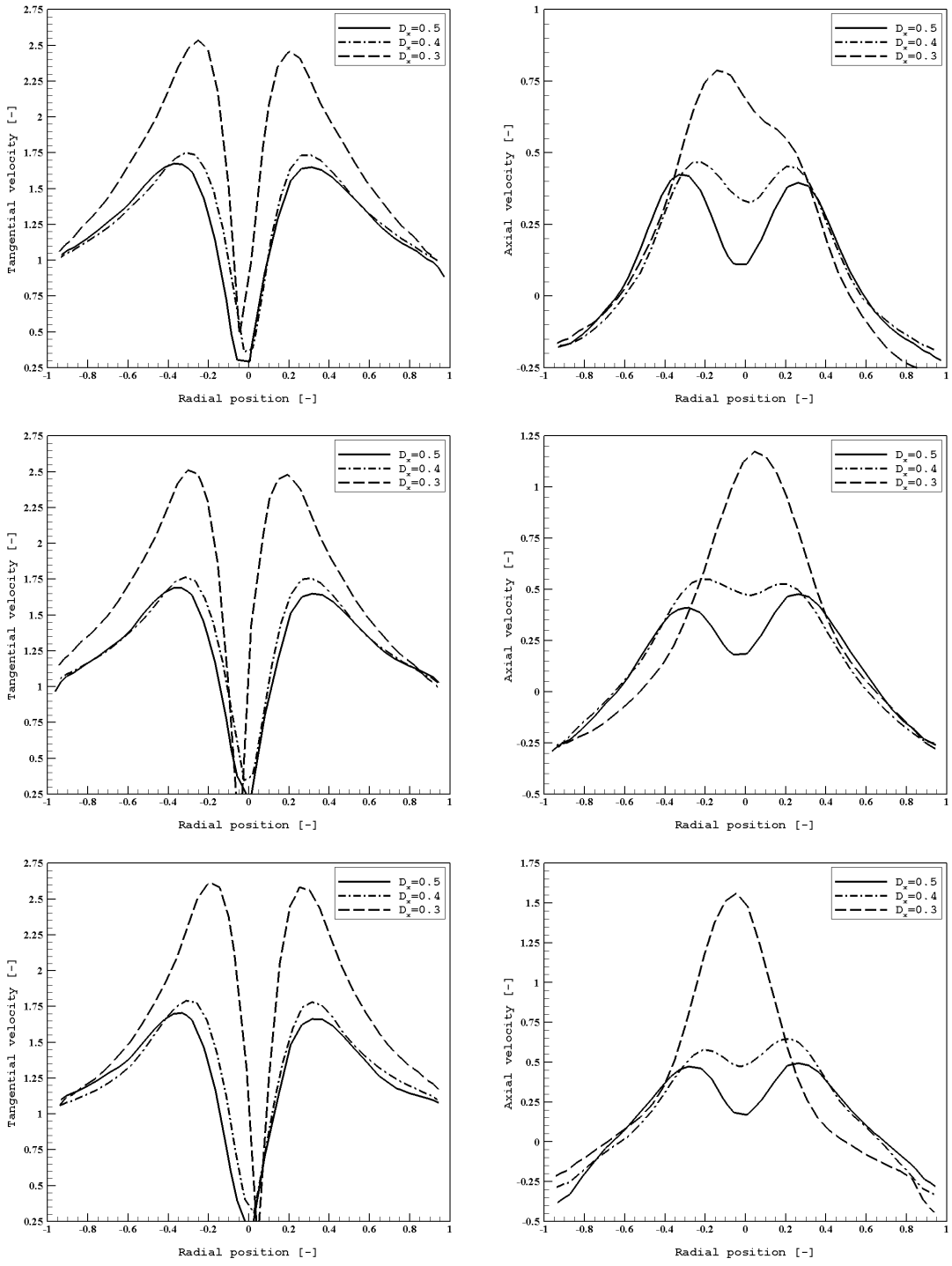

Figure 5: The radial profile for the time averaged tangential and axial velocity at different sections on the X-Z plane (Y=0) at sections S4 till S6 . From top to bottom: section S4 through section S6. From left to right: tangential velocity and axial velocity respectively.

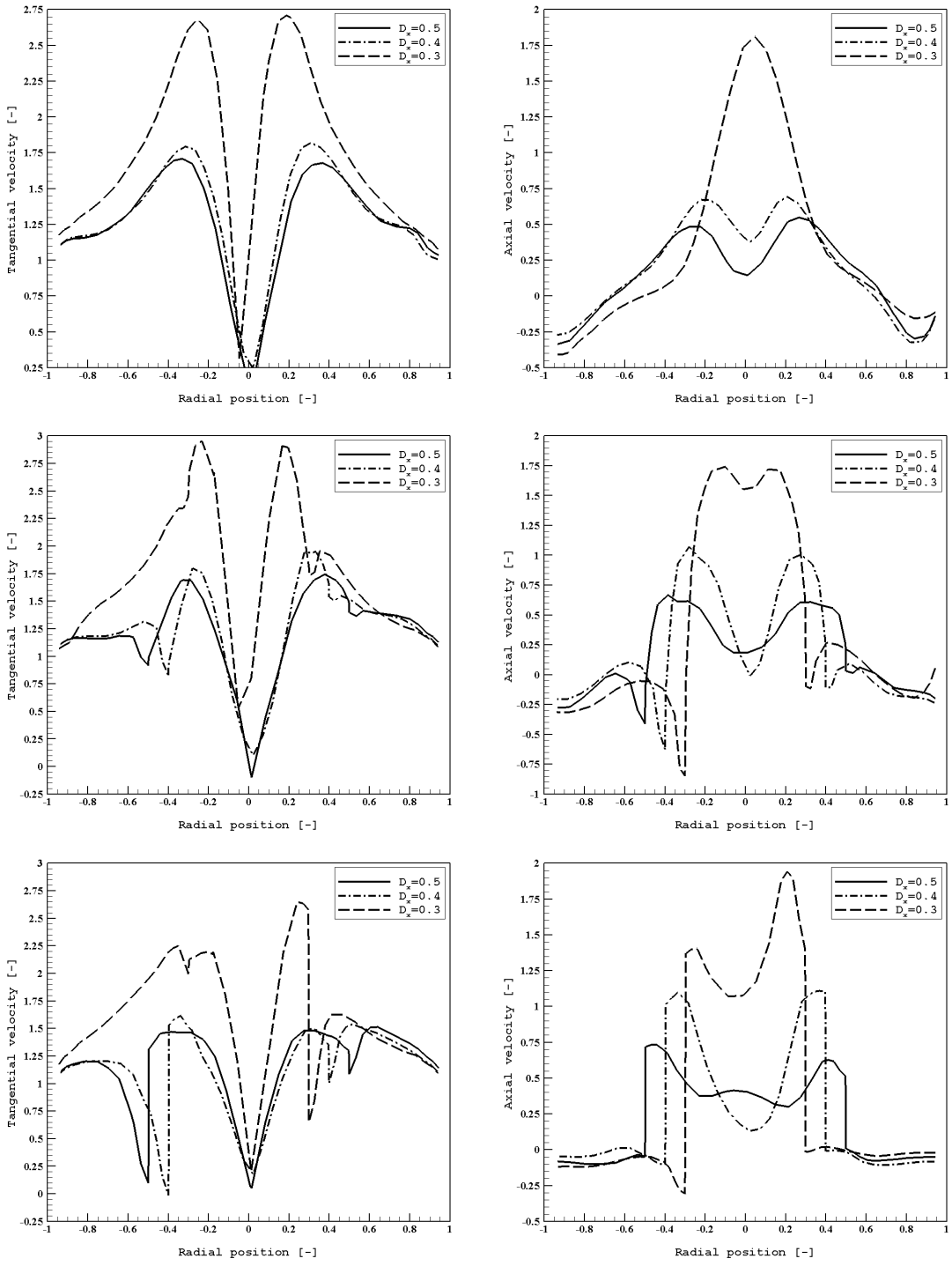

Figure 6: The radial profile for the time averaged tangential and axial velocity at different sections on the X-Z plane (Y=0) at sections S7 till S9 . From top to bottom: section S7 through section S9. From left to right: tangential velocity and axial velocity respectively.

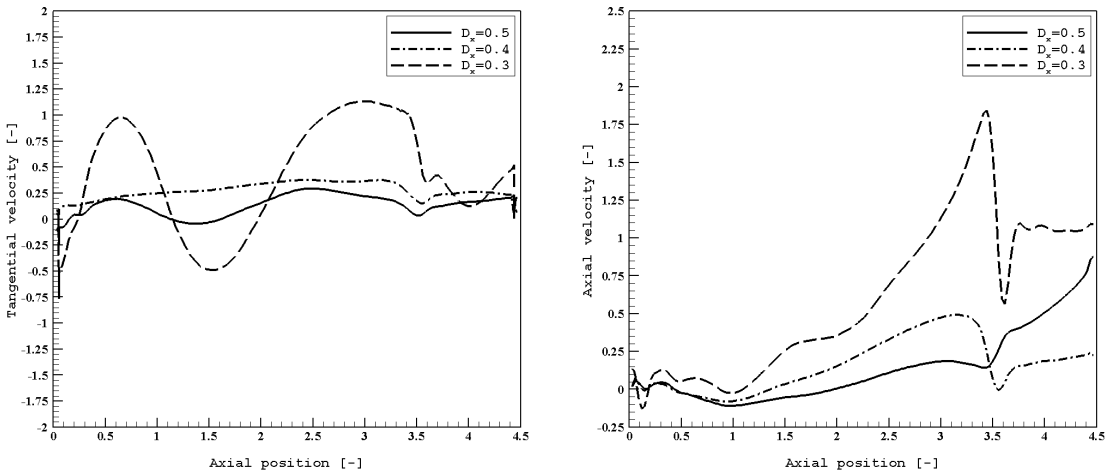

Figure 7: The axial profile for the time averaged tangential and axial velocity at centerline. From left to right: tangential velocity and axial velocity respectively.

ticles through the calculated flow field. The dispersed phase can exchange momentum, mass, and energy with the fluid phase.

A fundamental assumption made in this model is that the dispersed second phase occupies a low volume fraction (usually less than 10–12 %, where the volume fraction is the ratio between the total volume of particles and the volume of fluid domain), even though high mass loading is acceptable. The particle trajectories are computed individually at specified intervals during the fluid phase calculation. This makes the model appropriate for the modeling of particle-laden flows. The particle loading in a cyclone separator is small (3-5 %), and therefore, it can be safely assumed that the presence of the particles does not affect the flow field (one-way coupling).

In FLUENT, the drag coefficient for spherical particles is calculated by using the correlations developed by Morsi and Alexander.[17] The equation of motion for particles was integrated along the trajectory of an individual particle. Collection efficiency statistics were obtained by releasing a specified number of mono-dispersed particles at the inlet of the cyclone and by monitoring the number escaping through the outlet. Collisions between particles and the walls of the cyclone were assumed to be perfectly elastic (coefficient of restitution is equal to 1).

3.3.1 The DPM results

In order to calculate the effect of the vortex finder diameter on the cut-off size, 14280 particles were injected from the inlet surface with zero velocity and a mass flow rate $\dot{m}_p$ of 0.001 kg/s (corresponding to inlet dust concentration $C_{in}\dot{m}_p/Q_{in} = 11.89\ gm/m^3$) for each of the three cyclones. The particle density is 860 kg/m^3 and the maximum number of time steps for each injection was 900000 steps. The DPM analysis results for the three

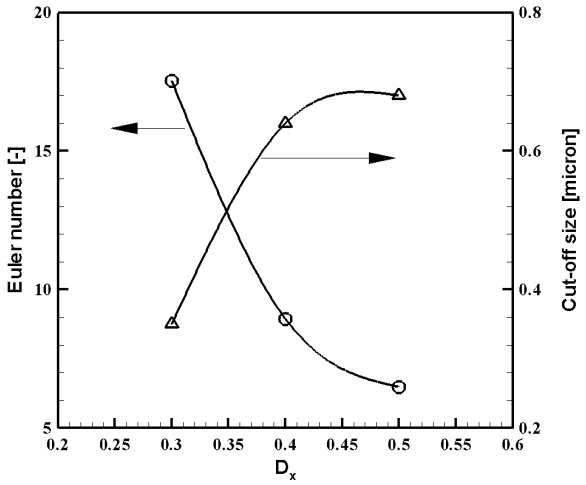

Figure 8: The effect of vortex finder diameter on the pressure drop(Euler number) and cut-off size(with spline curve fitting to get a smooth curve).

cyclones are depicted in Table 3 and Fig. 8. It is found that the cut off size decreases with decreasing the vortex finder while the pressure drop is increasing. Consequently for an optimal design of a cyclone separator a multi objective optimization should be used.

4 Conclusions

A Reynolds stress model has been used to study the effect of vortex finder diameter on the cyclone flow field and performance. Three cyclones with different values of D_x viz. 0.5,0.4, and 0.3 have been investigated. The following conclusion can been drawn.

- The vortex finder diameter has a significant effect on the flow pattern and performance.
- As vortex finder diameter decreases, the maximum tangential velocity increases, while its position is almost the same (around one third of the cyclone radius).
- The flow pattern and performance parameters of the first two cyclones I and II are

Table 3: The cut-off size and pressure drop for the three cyclones

Cyclone	I	II	III
Cut-off size $[\mu m]$	0.68	0.64	0.35
Pressure drop ΔP $[N/m^2]$	324.7	447	877
Euler number Eu $[\Delta P/(0.5\rho V_{in}^2)]$	6.48	8.94	17.54

very close while it is completely different from that of cyclone III with the narrowest vortex finder diameter ($D_x = 0.3$).

- The axial velocity profile of cyclone III is completely different from that of the other two cyclones at the cylindrical pattern and through the vortex finder.
- Decreasing the vortex finder diameter increases the asymmetry of the flow pattern.
- decreasing the vortex finder diameter increases the pressure drop slightly at the beginning, afterwards the change becomes more sharp. The reverse trend is obtained for the cut-off size. Consequently for an optimum value of vortex finder diameter a multi-objective optimization is needed.

REFERENCES

[1] B.E. Saltzman and J.M. Hochstrasser. Design and performance of miniature cyclone for respirable aerosol sampling. *Environmental Science & Technology*, 17(7):418–424, July 1983.

[2] J. Dirgo and D. Leith. Cyclone collection efficiency: Comparison of experimental results with theoretical predictions. *Aerosol Science and Technology*, 4:401–415, 1985.

[3] J. Dirgo and D. Leith. Performance of theoretically optimized cyclones. *Filtration & separation*, 22(2):119–125, 1985.

[4] D. L. Iozia and D. Leith. Effect of cyclone dimensions on gas flow pattern and collection efficiency. *Aerosol Science and Technology*, 10(3):491–500, 1989.

[5] D. L. Iozia and D. Leith. The logistic function and cyclone fractional efficiency. *Aerosol Science and Technology*, 12(3):598–606, 1990.

[6] G. Ramachandran, D. Leith, J. Dirgo, and H. Feldman. Cyclone optimization based on a new empirical model for pressure drop. *Aerosol Science and Technology*, 15: 135–148, 1991.

[7] M. E. Moore and A. R. McFarland. Performance modeling of single-inlet aerosol sampling cyclones. *Environmental Science and Technology*, 27(9):1842–1848, September 1993.

[8] Y. Zhu and K. W. Lee. Experimental study on small cyclones operating at high flow rates. *Journal of Aerosol Science*, 30:1303–1315, 1999.

[9] R. Xiang and K. W. Lee. Exploratory study on cyclones of modified designs. *Particulate Science and Technology*, 19(4):327–338, 2001.

[10] J. C. Kim and K. W. Lee. Experimental study of particle collection by small cyclones. *Aerosol Science and Technology*, 12:1003–1015, 1990.

[11] A. J. Hoekstra. *Gas flow field and collection efficiency of cyclone separators*. PhD thesis, Technical University Delft, 2000.

[12] K.S. Lim, H.S. Kim, and K.W. Lee. Characteristics of the collection efficiency for a cyclone with different vortex finder shapes. *Journal of Aerosol Science*, 35(6): 743–754, 2004.

[13] Arman Raoufi, Mehrzad Shams, Meisam Farzaneh, and Reza Ebrahimi. Numerical simulation and optimization of fluid flow in cyclone vortex finder. *Chemical Engineering and Processing*, 47:128–137, 2008.

[14] W. D. Griffiths and F. Boysan. Computational fluid dynamics (cfd) and empirical modelling of the performance of a number of cyclone samplers. *Journal of Aerosol Science*, 27(2):281–304, 1996.

[15] T.G. Chuah, J. Gimbun, and Thomas S.Y. Choong. A cfd study of the effect of cone dimensions on sampling aerocyclones performance and hydrodynamics. *Powder Technology*, 162:126 – 132, 2006.

[16] M. D. Slack, R. O.Prasad, A.Bakker, and F.Boysan. Advances in cyclone modeling using unstructured grids. *Trans IChemE.*, 78 Part A, November 2000.

[17] S. A. Morsi and A. J. Alexander. An investigation of particle trajectories in two-phase flow systems. *Journal of Fluid Mechanics*, 55(02):193–208, 1972.